Received: 12 July 2017 | Revised: 25 September 2017 | Accepted: 26 September 2017

DOI: 10.1002/aoc.4149

FULL PAPER

WILEY Applied Organometallic Chemistry

Synthesis, spectroscopic evaluation, molecular modelling, thermal study and biological evaluation of manganese(II) complexes derived from bidentate N,O and N,S donor Schiff base ligands

Savita Bargujar[1] | Sulekh Chandra[2] | Reeta Chauhan[2] | Hament K. Rajor[1] | Jyoti Bhardwaj[3]

[1] Department of Chemistry, Ramjas College, University of Delhi, Delhi 110 007, India

[2] Department of Chemistry, Zakir Husain Delhi College (Delhi University), JLN Marg, New Delhi 110 002, India

[3] Division of Plant Exploration and Germplasm Collection, NBPGR, Pusa, New Delhi 110012, India

Correspondence
Sulekh Chandra, Department of Chemistry, Zakir Husain Delhi College (Delhi University), JLN Marg, New Delhi 110 002, India.
Email: schandra_00@yahoo.com

Funding information
University Grants Commission, Grant/Award Number: 8-3(19)/2011 (MRP/NRCB) dated 20/12/2011

Manganese(II) complexes having the general composition $Mn(L)_2X_2$ (where L = 3-bromoacetophenone semicarbazone, 3-bromoacetophenone thiosemicarbazone, 1-tetralone semicarbazone, 1-tetralone thiosemicarbazone, flavanone semicarbazone or flavanone thiosemicarbazone and X = Cl^- or ½SO_4^{2-}) were synthesized. All the complexes were characterized using elemental analyses, molar conductance and magnetic moment measurements, and mass, ^1H NMR, infrared, electron paramagnetic resonance and electronic spectral studies. The molar conductance of the complexes in dimethylsulfoxide lies in the range 10–20 Ω^{-1} cm^2 mol^{-1} indicating their non-electrolytic nature. All the complexes show magnetic moments corresponding to five unpaired electrons. The possible geometries of the complexes were assigned on the basis of electron paramagnetic resonance, electronic and infrared spectral studies. Some of the synthesized ligands and their complexes were screened for their antifungal activities against fungi *Macrophomina phaseolina*, *Botrytis cinerea* and *Phoma glomerata* using the food poison technique and their antibacterial activities against *Xanthomonas campestris* pv. *campestris* and *Ralstonia solanacearum* using the paper disc diffusion method. They showed appreciable activities.

KEYWORDS
antifungal and antibacterial activities, bidentate, manganese(II) complexes, semicarbazone, thiosemicarbazone

1 | INTRODUCTION

Schiff base ligands are known for their excellent coordinating properties and hence exhibit variety in the structure of their metal complexes.[1] Schiff bases derived from thiosemicarbazide and semicarbazide moieties are an important class of compounds which have long attracted attention, owing to their notable biological and pharmacological properties.[2,3] Schiff bases are also used as catalysts, intermediates in organic synthesis, pigments, dyes, polymeric stabilizers and corrosion inhibitors.[4] It is also known that N and S donor atoms of Schiff bases play an important role in coordination of metals at the active sites of numerous metallobiomolecules.[5] Complexes of thiosemicarbazones with transition metals have received considerable attention because of their wide range of biological activities that include anti-tumour, antibacterial, fungicidal and anti-carcinogenic properties.[6–12] The well-documented biological activities of several thiosemicarbazones often have been attributed to

their ability to form chelates with transition metal ions.[13,14]

Mn(II) coordination compounds are very abundant in soil[15,16] and are essential for plant growth. In soil, these are formed by biodegradation of lignin.[17] Mn(II) was found to be important for enzymatic systems with DNA. DNA and RNA polymerases [18] catalyse the replication and transcription of DNA and have a specific requirements for Mn(II).[19] The complexes of Mn(II) play an important role in catalytic properties.[20]

In view of these applications, we have synthesized a series Schiff bases derived from semicarbazide and thiosemicarbazide moieties. These Schiff bases are further complexed with Mn(II) metal ion. Further structure elucidation and investigation of biological activities have been performed. In this paper we report the synthesis, characterization and biological evaluation of Mn(II) complexes with six bidentate N,O and N,S donor Schiff base ligands (Figure 1).

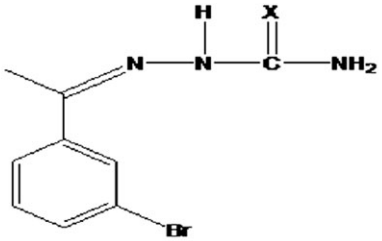

Where X=O, 3-Bromoacetophenone semicarbazone (L_1)

X=S, 3-Bromoacetophenone thiosemicarbazone (L_2)

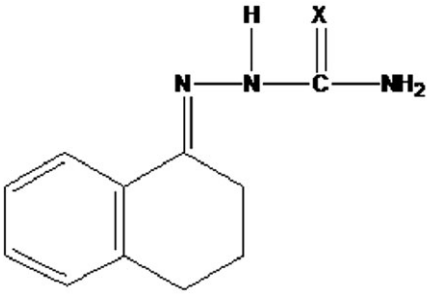

Where X=O, 1-Tetralone semicarbazone (L_3)

X=S, 1- Tetralone thiosemicarbazone (L_4)

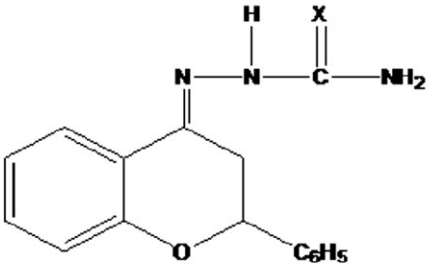

Where X=O, Flavanonesemicarbazone (L_5)

X=S, Flavanonethiosemicarbazone (L_6)

FIGURE 1 Structures of ligands

2 | EXPERIMENTAL

2.1 | Materials and methods

All the chemicals used were of AR grade and procured from Sigma Aldrich. Metal salts were purchased from E. Merck and were used as received. Fungal species were obtained from ITCC, Indian Agricultural Research Institute, New Delhi, and Plant Quarantine Division of National Bureau of Plant Genetic Resources, Pusa, New Delhi. Antifungal activities and antibacterial activities were evaluated using the food poison technique and disc diffusion method, respectively.

2.2 | Synthesis of ligands

All the ligands were prepared using methods reported earlier[21a] by coupling of semicarbazide hydrochloride and thiosemicarbazide with the corresponding ketones (Table 1).

2.3 | Preparation of complexes

A hot ethanolic (20 ml) solution of corresponding metal salt (0.001 mol) was mixed with a hot ethanolic solution of the corresponding ligands (0.002 mol).[21b] The mixture was refluxed at 80 ± 5 °C for 3–36 h. On cooling the contents, the complexes were precipitated out. These were filtered, washed with 50% ethanol and dried in vacuum over P_4O_{10}.

3 | ANALYSIS

3.1 | Physical measurements (Table 2)

Contents of C and H were analysed with a Carlo-Erba 1106 elemental analyser. The nitrogen content of the complexes was determined using Kjeldahl's method. Molar conductance was measured with an ELICO (CM82T) conductivity bridge. Magnetic susceptibilities were measured at room temperature with a Gouy balance using $CuSO_4{\cdot}5H_2O$ as calibrant. Electron impact mass spectra were recorded with a JEOL JMS-DX-303 mass spectrometer. Proton (^1H) NMR spectra were recorded with a Hitachi FT-NMR model R-600 spectrometer using deuterated dimethylsulfoxide (DMSO-d_6) as a solvent at 300 MHz. Chemical shifts were measured relative to tetramethylesilane. Fourier

TABLE 1 Schematic representation of synthesis of ligands L_1–L_6 from respective ketones and semicarbazide and thiosemicarbazide

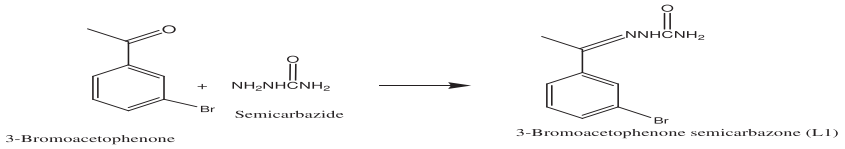

Synthesis of ligand 3-Bromoacetophenone semicarbazone (L_1)

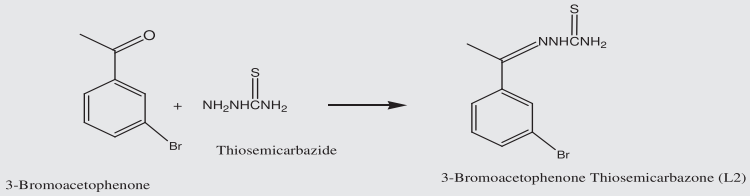

Synthesis of ligand 3-Bromoacetophenone Thiosemicarbazone (L_2)

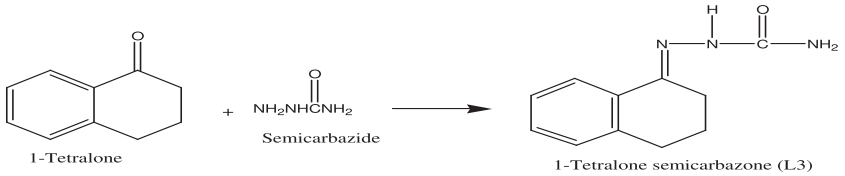

Synthesis of ligand 1-Tetralone semicarbazone (L_3)

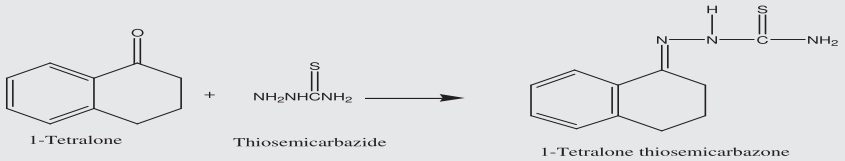

Synthesis of ligand 1-Tetralone thiosemicarbazone (L_4)

Synthesis of ligand Flavanone semicarbazone (L_5)

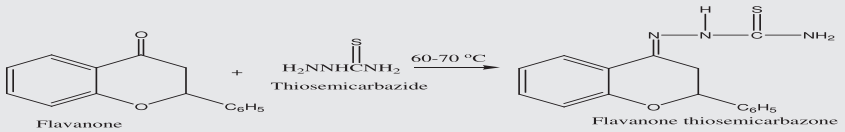

Synthesis of ligand Flavanone thiosemicarbazone (L_6)

transform infrared (FT-IR) spectra (CsI) were recorded with an FT-IR spectrum BX-II spectrophotometer. The electronic spectra were recorded in DMSO with a Shimadzu UV mini-1240 spectrophotometer. Electron paramagnetic resonance (EPR) spectra of the Mn(II) complexes were recorded as polycrystalline samples at room temperature with an E_4-EPR spectrometer using DPPH as the g-marker. The molecular weights of complexes were determined cryoscopically in benzene.

All the characterization work was done at the University Science Instrumentation Centre (USIC), University of Delhi, except EPR and NMR studies which were carried out at SAIF, IIT Bombay, Powai, Mumbai. NMR studies were carried out at IIT Delhi.

3.2 | Molecular modelling

HyperChem version 7.51 was used to perform molecular modelling of the ligands and their corresponding metal

complexes. It was used to determine energy values and other parameters like bond lengths and bond angles by first molecular mechanics MM plus force field and then semi-empirical method PM3 (parametric 3). Each time, a convergence limit was reached to 0.010 by setting up a criterion of RMS gradient of 0.100 kcal $Å^{-1}$ mol^{-1} and Polak–Ribiere optimization algorithm. Hydrogen atoms were omitted for clarity. Several cycles of energy minimization had to be carried out for each complex.

3.3 | *In Vitro* screening for antifungal activity

The preliminary fungitoxicity screening of the compounds at various concentrations was performed *in vitro* against the fungi *Macrophomina phaseolina*, *Botrytis cinerea* and *Phoma glomerata* using the food poison technique.[22] Fungal culture of *B. cinerea* was obtained from Indian Type Culture Collection, Indian Agricultural Research Institute, New Delhi (ITCC no. 6192) and *P. glomerata* was isolated from seeds of *Impatiens glandulifera* received from the UK in the Plant Quarantine Division of National Bureau of Plant Genetic Resources, New Delhi, by incubation on blotter. The mycelial growth of fungi (mm) in each Petri plate was measured diametrically and growth inhibition (I) was calculated using the formula

$$I\,(\%) = \frac{C-T}{C}\times 100$$

where C is the radial diameter of colony of control and T the radial diameter of colony of test compound.

3.4 | *In Vitro* screening for antibacterial activity

The antibacterial activities of the ligands and their metal complexes were evaluated against *Xanthomonas campestris* pv. *campestris* and *Ralstonia solanacearum* using the paper disc diffusion method.[6] Cultures of these bacteria were obtained from the Indian Agricultural Research Institute, New Delhi. Nutrient agar medium was used. Filter paper disc treated with DMSO served as control and with streptomycin used as a standard antibiotic. All determinations were made in duplicate for each of the compounds. An average of two independent readings for each compound was recorded. The Petri plates were kept in a refrigerator for 24 h for pre-diffusion. Finally, Petri plates were incubated for 26–30 h at 28 ± 2 °C. The zone of inhibition was measured carefully.

4 | RESULTS AND DISCUSSION

The molar conductance data (Table 2) of these complexes in DMSO indicated that they are non-electrolyte in nature.[23] Therefore, the complexes may be formulated as $[Mn(L)_2X_2]$ ($X = Cl^-$ or $½SO_4^{2-}$), where L = L_1, L_2, L_3, L_4, L_5 or L_6.

4.1 | FT-IR spectra of ligands

The FT-IR spectra of all the ligands showed bands in the range 3292–3499 and 3142–3197 cm^{-1} corresponding to the $\nu_{as}(NH_2)$ and $\nu_{as}(NH)$ stretching vibrations, respectively, showing the presence of NH_2 and NH groups in the ligands.

The FT-IR spectra of the semicarbazide-based ligands (L_1, L_3 and L_5) also showed bands in the range 1690–1708 and 1571–1583 cm^{-1} which may be assigned to ν(C=O) and ν(C=N) stretching vibrations, respectively, while the FT-IR spectra of the thiosemicarbazide-based ligands (L_2, L_4 and L_6) showed bands in the range 1585–1601 and 762–852 cm^{-1} which may be assigned to ν(C=N) and ν(C=S) stretching vibrations, respectively. On complexation, the positions of bands due to ν(>C=N) and ν(>C=O) in L_1, L_3 and L_5 and due to ν(>C=N) and ν(>C=S) in L_2, L_4 and L_6 are shifted by 10–60 cm^{-1}. This indicated that in the case of semicarbazone complexes the coordination takes place through the nitrogen atoms of imine group and oxygen atom of the >C=O group, while in the case of thiosemicarbazone complexes the coordination takes place through nitrogen atoms of the imine group and sulfur atom of the >C=S group. Hence all the ligands behave as bidentate ones.[24,25]

4.2 | ^{1}H NMR spectra of ligands

^{1}H NMR spectra of the ligands were recorded in DMSO-d_6 at 300 MHz (Figure 2). The non-equivalent protons were found to resonate at different values of applied field.

4.2.1 | Ligand L_1

A singlet appeared at 9.415 ppm attributed to one proton of NH, a singlet at 6.590 ppm was observed for two protons of NH_2, a singlet at 2.173 ppm was due to 3H of CH_3 group and a multiplet observed between 7.305 and 8.072 ppm was attributed to aromatic protons.

4.2.2 | Ligand L_2

A singlet appeared at 8.760 ppm for one proton of NH, a singlet at 6.461 ppm was observed for two protons of

TABLE 2 Colour, molar conductance and elemental analyses of Mn(II) complexes

Complex	Color	Molecular weight	Molar conductance	Yield (%)	Elemental analysis: found (calcd)			
					M (%)	C (%)	H (%)	N (%)
$[Mn(L_1)_2Cl_2]$	Pink	635.9	10.7	62	8.57	33.90	3.08	13.09
$MnC_{18}H_{20}N_6O_2Br_2Cl_2$					(8.63)	(33.97)	(3.15)	(13.21)
$[Mn(L_1)_2SO_4]$	Pink	660.9	12.1	61	8.27	32.59	2.94	12.67
$MnC_{18}H_{20}N_6O_6Br_2S$					(8.31)	(32.68)	(3.03)	(12.71)
$[Mn(L_2)_2Cl_2]$	White	667.9	10.8	57	8.17	32.29	2.92	12.78
$MnC_{18}H_{20}N_6Br_2S_2Cl_2$					(8.22)	(32.34)	(2.99)	(12.86)
$[Mn(L_2)_2SO_4]$	White	692.9	10.1	59	7.87	31.13	2.89	12.07
$MnC_{18}H_{20}N_6O_4Br_2S_3$					(7.92)	(31.17)	(2.81)	(12.12)
$[Mn(L_3)_2Cl_2]$	White	531.9	12.5	52	10.26	49.52	4.81	15.72
$MnC_{22}H_{26}N_6O_2Cl_2$					(10.32)	(49.63)	(4.89)	(15.79)
$[Mn(L_3)_2SO_4]$	White	556.9	13.1	54	9.78	47.33	4.61	15.01
$MnC_{22}H_{26}N_6O_6S$					(9.86)	(47.41)	(4.67)	(15.08)
$[Mn(L_4)_2Cl_2]$	White	563.9	11.3	53	9.71	46.78	4.54	14.87
$MnC_{22}H_{26}N_6S_2Cl_2$					(9.74)	(46.82)	(4.61)	(14.90)
$[Mn(L_4)_2SO_4]$	White	588.9	15.4	56	9.25	44.79	4.37	14.23
$MnC_{22}H_{26}N_6O_4S_3$					(9.32)	(44.83)	(4.42)	(14.26)
$[Mn(L_5)_2Cl_2]$	Yellow	687.9	14.8	52	7.93	55.74	4.31	12.14
$MnC_{32}H_{30}N_6O_4Cl_2$					(7.98)	(55.82)	(4.36)	(12.21)
$[Mn(L_5)_2SO_4]$	White	712.9	15.2	54	7.74	53.81	4.18	11.71
$MnC_{32}H_{30}N_6O_8S$					(7.70)	(53.86)	(4.21)	(11.78)
$[Mn(L_6)_2Cl_2]$	White	719.9	13.6	54	7.59	53.31	4.13	11.62
$MnC_{32}H_{30}N_6O_2S_2Cl_2$					(7.63)	(53.34)	(4.17)	(11.67)
$[Mn(L_6)_2SO_4]$	White	744.9	14.9	55	7.32	51.58	4.07	11.21
$MnC_{32}H_{30}N_6O_6S_3$					(7.37)	(51.55)	(4.03)	(11.28)

NH_2, a singlet at 1.650 ppm was due to 3H of CH_3 group and a multiplet observed between 7.266 and 7.860 ppm was attributed to aromatic protons.

4.2.3 | Ligand L_3

A singlet appeared at 9.280 ppm for one proton of NH, a singlet at 6.527 ppm was observed for two protons of NH_2 and a multiplet observed between 7.132 and 7.244 ppm was attributed to aromatic protons.

4.2.4 | Ligand L_4

A singlet appeared at 10.139 ppm for one proton of NH, a singlet at 6.005 ppm was observed for two protons of NH_2 and a multiplet observed between 7.169 and 7.283 ppm was attributed to aromatic protons.

4.2.5 | Ligand L_5

A singlet appeared at 9.511 ppm for one proton of NH, a singlet at 6.616 ppm was observed for two protons of NH_2 and a multiplet observed between 6.950 and 8.226 ppm was attributed to aromatic protons.

4.2.6 | Ligand L_6

A singlet appeared at 8.658 ppm for one proton of NH, a singlet at 6.369 ppm was observed for two protons of NH_2 and a multiplet observed between 7.008 and 7.975 ppm was attributed to aromatic protons.

4.3 | Electron impact mass spectra of ligands

The electron impact mass spectra of the ligands showed molecular ion peaks at m/z = 255, 271, 203, 219, 281

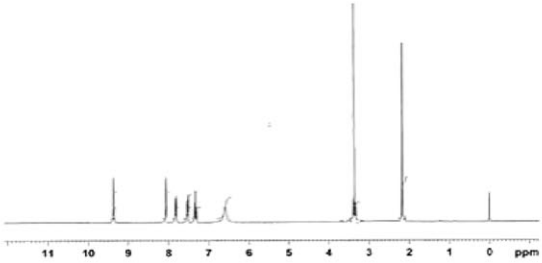

^{1}H NMR spectrum of ligand 3-Bromoacetophenone semicarbazone (L_1)

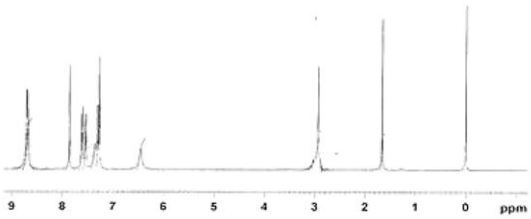

^{1}H NMR spectrum of ligand 3-Bromoacetophenone thiosemicarbazone (L_2)

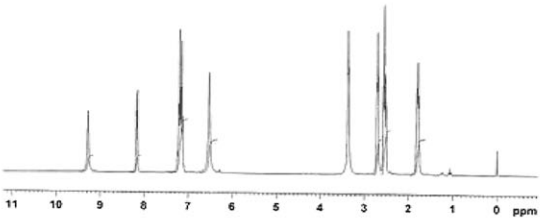

^{1}H NMR spectrum of ligand 1-Tetralone semicarbazone (L_3)

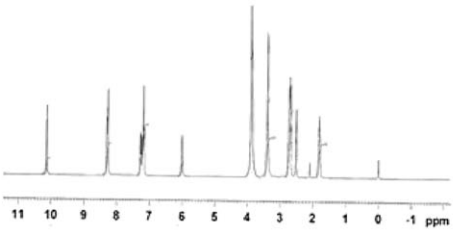

^{1}H NMR spectrum of ligand 1-Tetralone thiosemicarbazone (L_4)

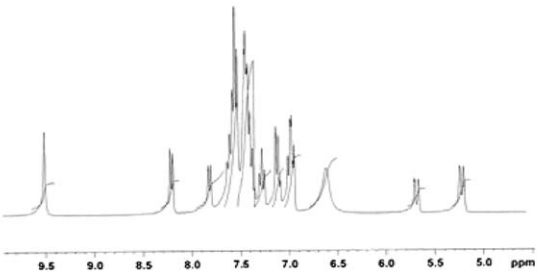

^{1}H NMR spectrum of ligand Flavanonesemicarbazone (L_5)

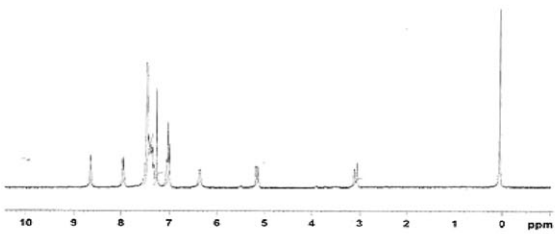

^{1}H NMR spectrum of ligand Flavanonethiosemicarbazone (L_6)

FIGURE 2 ^{1}H NMR spectra of ligands in DMSO-d_6

and 297 amu corresponding to species $[C_9H_{10}N_3OBr]^+$, $[C_9H_{10}N_3SBr]^+$, $[C_{11}H_{13}N_3O]^+$, $[C_{11}H_{13}N_3S]^+$, $[C_{16}H_{15}N_3O_2]^+$ and $[C_{16}H_{15}N_3OS]^+$, respectively, which confirmed the proposed formula of the ligands. These ligands also showed peaks corresponding to various fragments. The intensities of these peaks gave an indication of the stabilities of the fragments.

4.4 | Chloro complexes: $[Mn(L)_2Cl_2]$

Magnetic moments of these complexes lie in the range 5.81–5.97 BM corresponding to five unpaired electrons.[26] The electronic spectra of the complexes (Table 3) show four weak-intensity bands in the range 9681–19 201 cm^{-1} (ε = 32–38 l mol^{-1} cm^{-1}), 16 920–27 932 cm^{-1} (ε = 41–45 l mol^{-1} cm^{-1}), 21 413–30 487 cm^{-1} (ε = 75–88 l mol^{-1} cm^{-1}) and 27 173–34 965 cm^{-1} (ε = 138–149 l mol^{-1} cm^{-1}). These bands may be assigned to $^6A_{1g} \rightarrow {}^4T_{1g}$ (4G), $^6A_{1g} \rightarrow {}^4E_g$, $4A_{1g}$ (4G) (10B + 5C), $^6A_{1g} \rightarrow {}^4E_g$ (4D) (17B + 5C) and $^6A_{1g} \rightarrow {}^4T_{1g}$ (4P) (7B + 7C) transitions, respectively.[27]

4.5 | Sulfato complexes: $[Mn(L)_2SO_4]$

Room temperature magnetic moments of these complexes lie in the range 5.84–5.96 BM, these values being in tune with a high-spin configuration. The FT-IR spectra of the sulfato complexes show bands characteristic of bidentate sulfate group where ν_3 split at 1113–1194, 1054–1089 and 1021–1031 cm^{-1} while ν_1 at 903–990 cm^{-1} (Figure 3).[28] The molar conductance measurements of the sulfato complexes recorded at room temperature in DMSO solution were indicative of non-electrolyte behaviour.[23] The electronic spectra of the complexes (Table 3) recorded at room temperature in DMSO solution showed three bands in the range 9785–18 416 cm^{-1} (ε = 38–44 l mol^{-1} cm^{-1}), 17 825–23 052 cm^{-1} (ε = 73–86 l mol^{-1} cm^{-1}) and 22 272–27 248 cm^{-1} (ε = 136–149 l mol^{-1} cm^{-1}), which may be assigned to the transitions $^6A_{1g} \rightarrow {}^4T_{2g}$ (4G), $^6A_{1g} \rightarrow {}^4T_{2g}$ (4D) and $^6A_{1g} \rightarrow {}^4A_{2g}$ (4F), respectively.[29,30] These bands are characteristic for six-coordinated octahedral geometry for these complexes.

All the Mn(II) complexes show isotropic EPR spectra (Figure 4), when recorded as polycrystalline samples. The *g*-tensor values were calculated using the Kneubuhl method and the results are presented in Table 3. The parameters *B* and *C* were calculated from the second and third transitions because these transitions are free from the crystal field splitting and depend on *B* and *C* parameters.[31] The values of *Dq* were obtained with the help of a curve of transition energies versus *Dq*, as given by Orgel[32] using the energy due to the transition $^6A_{1g} \rightarrow {}^4T_{1g}$ (4G). Parameters *B* and *C* are linear combinations of certain Coulomb and exchange integral and are generally treated as empirical parameters obtained from the spectra of the free ions. Slater–Condon–Shortley repulsion parameters F_2 and F_4 are related to Racah parameters *B* and *C* as: $B = F_2 - 5F_4$ and $C = 35F_4$.

The electron–electron repulsion in the complexes is more than in the free ion, resulting in an increased distance between electrons, and thus affecting the size of the orbital. On increasing delocalization, the value of β decreases to less than one for the complexes. The value of β can be calculated from the nephelauxetic parameter for the ligand (*hx*) and the nephelauxetic parameter for

TABLE 3 Magnetic moments, electronic spectral data and EPR spectral data of Mn(II) complexes

Complex	μ_{eff} (BM)	λ_{max} (cm^{-1})	*Dq* (cm^{-1})	*B* (cm^{-1})	*C* (cm^{-1})	B	F_2 (cm^{-1})	F_4 (cm^{-1})	hx	g_{iso}
$[Mn(L_1)_2Cl_2]$	5.91	10 121, 18 622, 23 095, 32 573	703	639	2446	0.8	988	70	2.67	2.0018
$[Mn(L_1)_2SO_4]$	5.84	10 000, 17 825, 22 272, 30 864	699	635	2295	0.8	963	66	2.74	2.0014
$[Mn(L_2)_2Cl_2]$	5.81	18 622, 22 523, 26 525, 28 902	629	572	3361	0.7	1052	96	3.89	2.0019
$[Mn(L_2)_2SO_4]$	5.92	9785, 18 418, 22 626, 29 674, 32 258	661	601	2481	0.8	956	71	3.36	2.0017
$[Mn(L_3)_2Cl_2]$	5.97	9980, 17 953, 22 222, 34 843	671	610	2371	0.8	949	68	3.2	2.0021
$[Mn(L_3)_2SO_4]$	5.93	10 081, 18 622, 22 676, 34 602	637	579	2566	0.7	946	73	3.76	2.0022
$[Mn(L_4)_2Cl_2]$	5.96	9681, 16 920, 21 413, 34 965	706	642	2100	0.8	942	60	2.62	2.0015
$[Mn(L_4)_2SO_4]$	5.87	10 021, 18 727, 23 529, 28 653	755	686	2373	0.9	1025	68	1.82	2.0018
$[Mn(L_5)_2Cl_2]$	5.89	9709, 19 193, 23 310, 27 173, 28 248	647	588	2662	0.8	968	76	3.6	2.002
$[Mn(L_5)_2SO_4]$	5.92	18 330, 23 052, 25 157, 28 854	331	301	4009	0.4	873	115	8.82	2.0015
$[Mn(L_6)_2Cl_2]$	5.99	19 201, 27 932, 30 487, 28 916	402	365	4856	0.5	1059	139	7.65	2.0014
$[Mn(L_6)_2SO_4]$	5.96	18 416, 22 624, 27 248, 32 258	727	661	3204	0.8	1118	92	2.28	2.0016

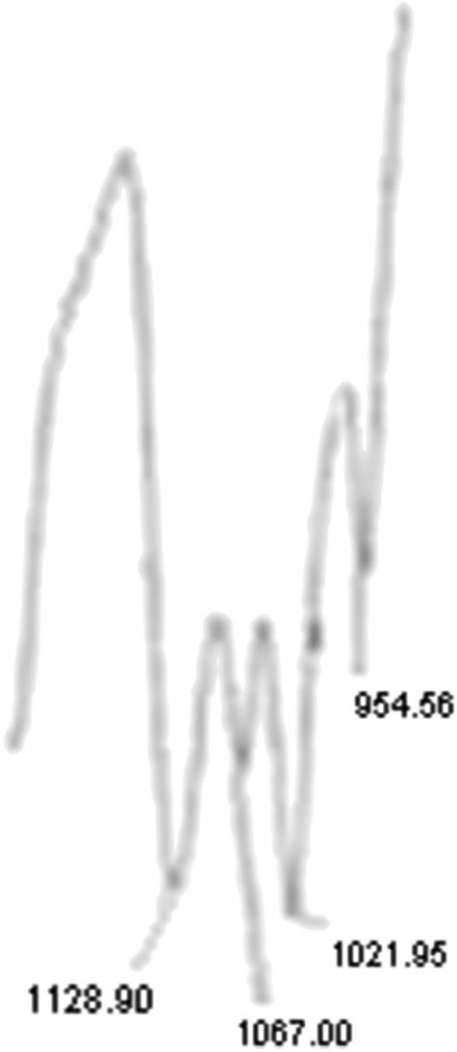

FIGURE 3 FT-IR spectrum of $[Mn(L_1)_2SO_4]$

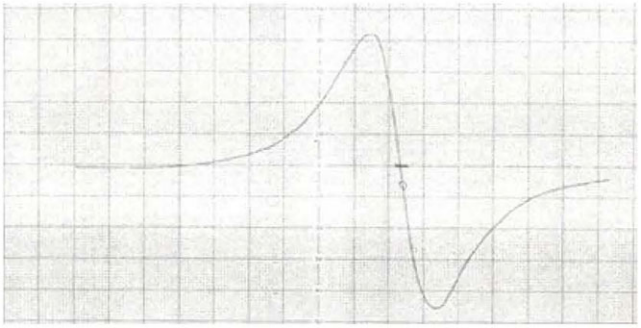

FIGURE 4 EPR spectrum of $[Mn(L_2)_2SO_4]$

the metal ion (km) as $(1 - \beta) = hx \times km$. The value of the parameter hx for Mn(II) complexes was calculated using the covalency contribution of Mn(II), while for the calculation of β, we used the numerical value of B for Mn(II) free ion which is 786 cm^{-1}. The observed values for β and hx suggest that the complexes, reported here, have

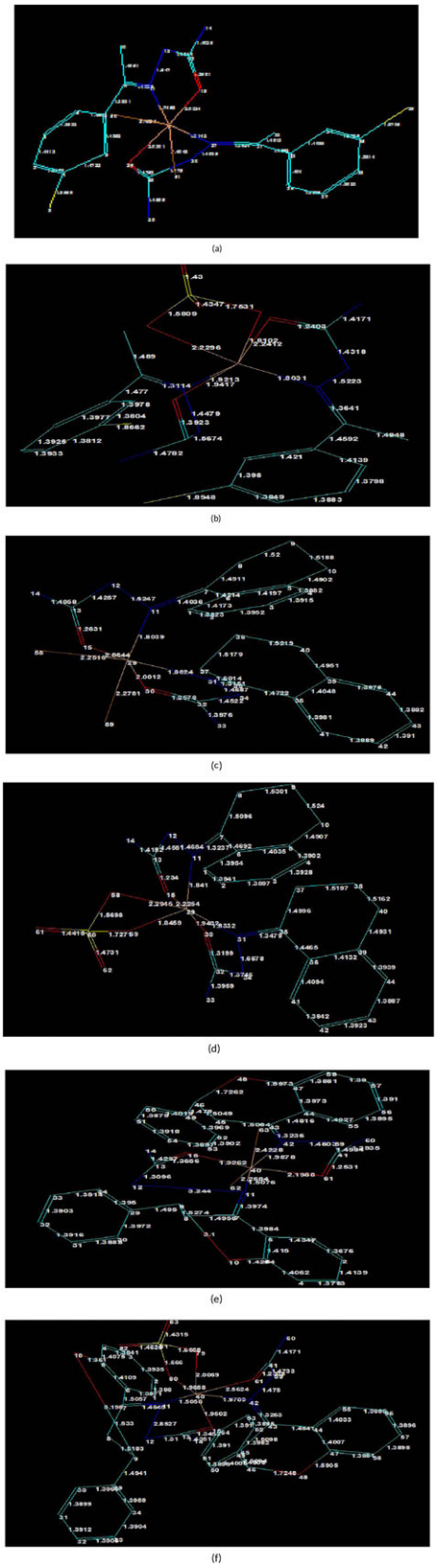

FIGURE 5 Energy minimized structures of (a) $Mn(L_1)_2Cl_2$, (b) $Mn(L_1)_2SO_4$, (c) $Mn(L_2)_2Cl_2$, (d) $Mn(L_2)_2SO_4$, (e) $Mn(L_3)_2Cl_2$ and (f) $Mn(L_3)_2SO_4$. Cyan, carbon; blue, nitrogen; orange, manganese; yellow, sulfur; yellow in phenyl ring, bromine; red, oxygen; grey, chlorine

TABLE 4 Energy values and bond angles of various manganese complexes

$Mn(L_1)_2Cl_2$ binding energy = −5140.0731 kcal mol^{-1}		$Mn(L_1)_2SO_4$ binding energy = −5514.0949 kcal mol^{-1}		$Mn(L_3)_2Cl_2$ binding energy = −6141.5077 kcal mol^{-1}		$Mn(L_3)_2SO_4$ binding energy = −6504.0722 kcal mol^{-1}		$Mn(L_5)_2Cl_2$ binding energy = −8370.1318 kcal mol^{-1}		$Mn(L_5)_2SO_4$ binding energy = −8806.6578 kcal mol^{-1}	
Atom no.	Bond angle (°)	Atom no.	Bond angle (°)	Atom no.	Bond angle (°)	Atom no.	Bond angle (°)	Atom no.	Bond angle (°)	Atom no.	Bond angle (°)
31–27–30	119.38	15–1–26	154.268	15–29–11	84.1079	15–29–11	82.4547	63–40–62	80.8067	79–40–80	72.0482
30–28–29	112.673	11–1–51	172.011	15–29–58	81.2371	15–29–58	99.6802	63–40–15	84.4299	61–40–42	70.6644
30–28–26	112.798	50–1–51	68.1334	58–29–59	95.2312	58–29–59	67.533	15–40–62	97.4776	42–40–15	82.9766
26–1–27	86.4187	51–1–26	73.4285	59–29–30	87.1547	59–29–30	116.335	62–40–11	97.7391	11–40–15	107.058
27–1–51	95.0702	26–1–27	72.0913	30–29–31	83.8445	30–29–31	90.2194	11–40–61	98.0252	11–40–80	105.741
51–1–15	90.6867	50–1–27	137.573	31–29–11	92.4102	31–29–11	118.951	61–40–42	87.0387	11–40–61	178.926
15–1–11	88.6937	27–1–11	96.9948	11–29–59	158.039	11–29–59	121.333	42–40–63	77.4126	79–40–15	149.842
15–1–50	78.9443	50–52–51	86.5768	31–29–58	168.612	58–29–31	163.647	15–13–14	115.356	80–40–42	144.772
50–1–51	72.7839	15–13–12	117.666	15–29–30	160.305	15–29–30	172.383	62–40–42	155.501	80–40–11	105.741
26–1–50	87.3493	12–11–9	114.312	12–13–14	121.661	15–29–31	84.1394	63–40–11	178.421	61–40–15	71.9221
27–1–50	167.177	27–30–28	104.345	15–13–12	118.509	11–29–31	118.957	15–40–61	166.681	79–40–42	94.7351
26–1–15	165.196	31–27–30	125.612	12–11–7	112.963	11–1213	114.86	13–12–62	72.8065	80–40–15	92.5943
51–1–11	162.196	12–13–15	117.666	31–34–32	110.482	14–13–15	122.266	12–11–7	92.2109	80–81–79	89.0338
15–13–12	120.978	30–28–26	104.062	30–32–33	118.894	58–60–59	89.8691	43–42–59	119.324	61–41–59	119.163
13–12–11	110.461			34–32–33	119.818	33–32–34	125.699	43–42–40	135.725	5–10–9	52.0516
9–11–12	115.83					30–32–33	116.213	8–9–10	67.9912	15–13–14	113.371
						34–31–35	114.946	47–48–46	116.767	59–42–43	119.115
								15–13–12	115.183	11–12–13	92.7307

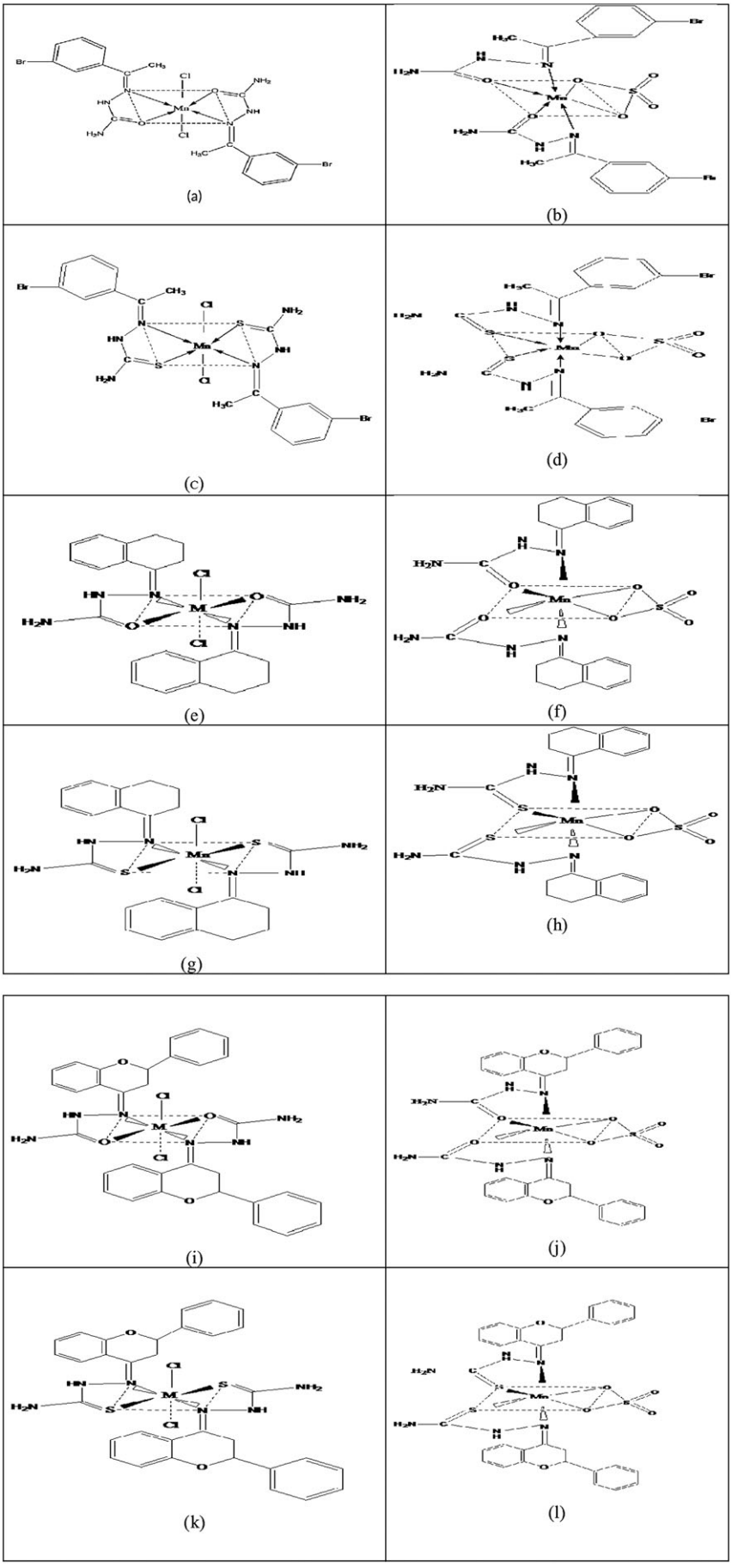

FIGURE 6 Proposed structures of complexes: (a) $[Mn(L_1)_2Cl_2]$; (b) $[Mn(L_1)_2SO_4]$; (c) $[Mn(L_2)_2Cl_2]$; (d) $[Mn(L_2)_2SO_4]$; (e) $[Mn(L_3)_2Cl_2]$; (f) $[Mn(L_3)_2SO_4]$; (g) $[Mn(L_4)_2Cl_2]$; (h) $[Mn(L_4)_2SO_4]$; (i) $[Mn(L_5)_2Cl_2]$; (j) $[Mn(L_5)_2SO_4]$; (k) $[Mn(L_6)_2Cl_2]$; (l) $[Mn(L_6)_2SO_4]$

appreciable ionic character.[33,34] The calculated values of the ligand field parameters are given in Table 3.

4.6 | Molecular modelling

As single crystals of the metal complexes could not be obtained, molecular modelling was done to obtain much structural information. Geometry optimization was done using HyperChem version 7.51[35] for L_1, L_3 and L_5 ligands and their complexes, i.e. $[Mn(L_1)Cl_2]$, $[Mn(L_1)SO_4]$, $[Mn(L_3)Cl_2]$, $[Mn(L_3)SO_4]$, $[Mn(L_5)Cl_2]$ and $[Mn(L_5)SO_4]$, while L_2, L_4 and L_6 complexes are not presented here as there is a sulfur atom in place of an oxygen atom of the ligands.

In order to obtain energy values and other structural details for these complexes we optimized the molecular structure of the complexes. Energy minimization was repeated several times by constraining the octahedral geometry to determine the global minimum. The energy minimized structures along with bond lengths are presented in Figure 5. The energy values and bond angles are presented in Table 4.

4.7 | Thermal study

The thermal stability of the Mn(II) complexes was studied by controlling heating rates at 10 °C min^{-1} under nitrogen atmosphere. Thermograms of Mn(II) complexes show two steps of decomposition and stable up to 250 °C, indicating the absence of lattice water as well as coordinated water. Generally in lattice water is lost at low temperature between 60 and 120 °C, whereas coordinated water requires 120–250 °C. Absence of water molecules in the Mn(II) complexes was supported by the differential thermal analysis (DTA) curves, which represented weight loss by endothermic bands. The DTA curves of Mn(II) complexes have no endothermic bands in the range 60–250 °C. Endothermic bands present at high temperature in DTA curves of Mn(II) complexes were due to loss of organic molecules and finally metal may convert into its oxide.[36,37] In addition to endothermic bands, the DTA curves of the complexes also show exothermic bands. These bands appeared at high temperature and represent phase transition, oxidation and/or decomposition of the complex. For the thermograms of the Mn(II) complexes attempts were not made to characterize the products formed at the end of the first stage. At the end of the second step, i.e. at 750 °C, stable manganese oxide was formed. The complexes are found to be thermally more stable than the corresponding Schiff base ligands.

On the basis of the above discussion, structures can be proposed for the synthesized complexes, as shown in Figure 6.

4.8 | *In Vitro* screening for antifungal activity

The antifungal screening data showed that the compounds exhibit antifungal properties, and it is also

TABLE 5 Fungal inhibition (%)

	M. phaseolina				*B. cinerea*				*P. glomerata*			
Compound	**500 μg ml^{-1}**	**800 μg ml^{-1}**	**1000 μg ml^{-1}**	**1500 μg ml^{-1}**	**500 μg ml^{-1}**	**800 μg ml^{-1}**	**1000 μg ml^{-1}**	**1500 μg ml^{-1}**	**500 μg ml^{-1}**	**800 μg ml^{-1}**	**1000 μg ml^{-1}**	**1500 μg ml^{-1}**
L_1	39	48	56	62	3.7	68	71	85	33	38	52	64
$[Mn(L_1)_2Cl_2]$	43	52	59	72	28	75	83	90	51	57	75	86
$[Mn(L_1)_2SO_4]$	62	67	80	90	49	83	94	100	57	65	84	91
L_2	45.83	54	61	75	5.4	74.7	—[a]	70	39.04	48	63	69
$[Mn(L_2)_2Cl_2]$	67	74	81	93	34	88	95	100	59	63	82	90
$[Mn(L_2)_2SO_4]$	70	78	92	97	55	91	100	100	65	72	94	97
L_3	34	55	60	71	51	65	72	84	53	64	67	80
$[Mn(L_3)_2Cl_2]$	48	61	68	77	62	70	80	92	60	75	81	87
$[Mn(L_3)_2SO_4]$	55	66	73	84	68	77	89	99	69	83	88	96
L_4	—	62.9	64	—	—	74.7	76	—	—	70.6	74	—
$[Mn(L_4)_2Cl_2]$	53	68	76	84	70	81	84	88	67	77	80	90
$[Mn(L_4)_2SO_4]$	58	71	83	95	81	96	100	100	76	85	93	98
Bavistin	90	100	100	100	26	51	62	71	86	100	100	100

[a]Not tested.

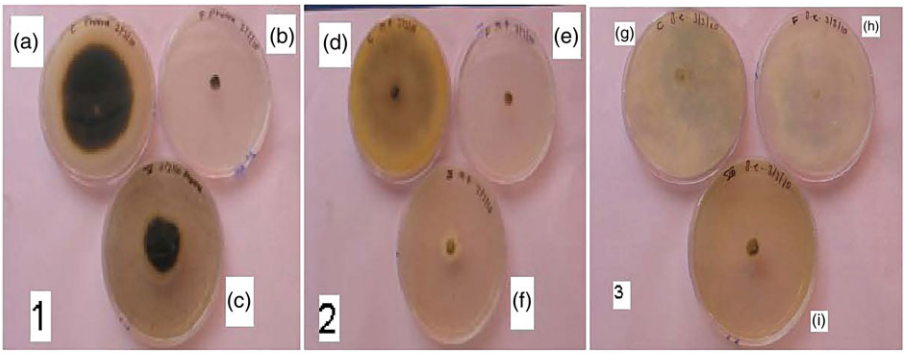

1: *Phoma glomerata* **2 :** *Macrophomina phaseolena* **3:** *Botrytis cinerea*
A: Control plate **B:** Bavistin at 800 μg ml^{-1} **C:** $[Mn(L_4)_2SO_4]$ 800 μg ml^{-1}

D: Control plate **E:** Bavistin at 1500 μg ml^{-1} **F:** $[Mn(L_4)_2SO_4]$ 1500 μg ml^{-1}

G: Control plate **H:** Bavistin at 1500 μg ml^{-1} **I:** $[Mn(L_4)_2SO_4]$ 1500 μg ml^{-1}

FIGURE 7 Plates showing antifungal activities

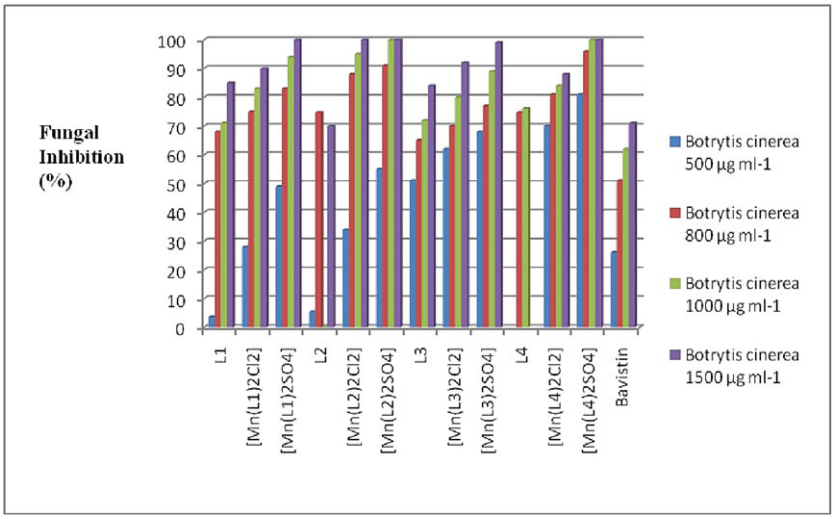

FIGURE 8 Activities of various ligands and complexes at different concentrations against the fungus *B. cinerea*

TABLE 6 Antibacterial screening data for ligands L_2 and L_4 their chloro and sulfato complexes

	Diameter of inhibition zone (mm)					
	X. campestris pv. *campestris*			R. solanacearum		
Compound	**250 μg ml^{-1}**	**500 μg ml^{-1}**	**1000 μg ml^{-1}**	**250 μg ml^{-1}**	**500 μg ml^{-1}**	**1000 μg ml^{-1}**
s	0	0	0	0	0	0
$[Mn(L_2)_2Cl_2]$	0	0	0	0	0	0
$[Mn(L_2)_2SO_4]$	18	20	24	17	19	25.3
L_4	0	0	0	0	0	0
$[Mn(L_4)_2Cl_2]$	0	0	0	0	0	11
$[Mn(L_4)_2SO_4]$	17.5	20	22	14	16.5	19.05
Streptomycin (standard)	19	22	26	26	30	—[a]
Solvent (DMSO)	0	0	0	0	0	0

[a]Not tested.

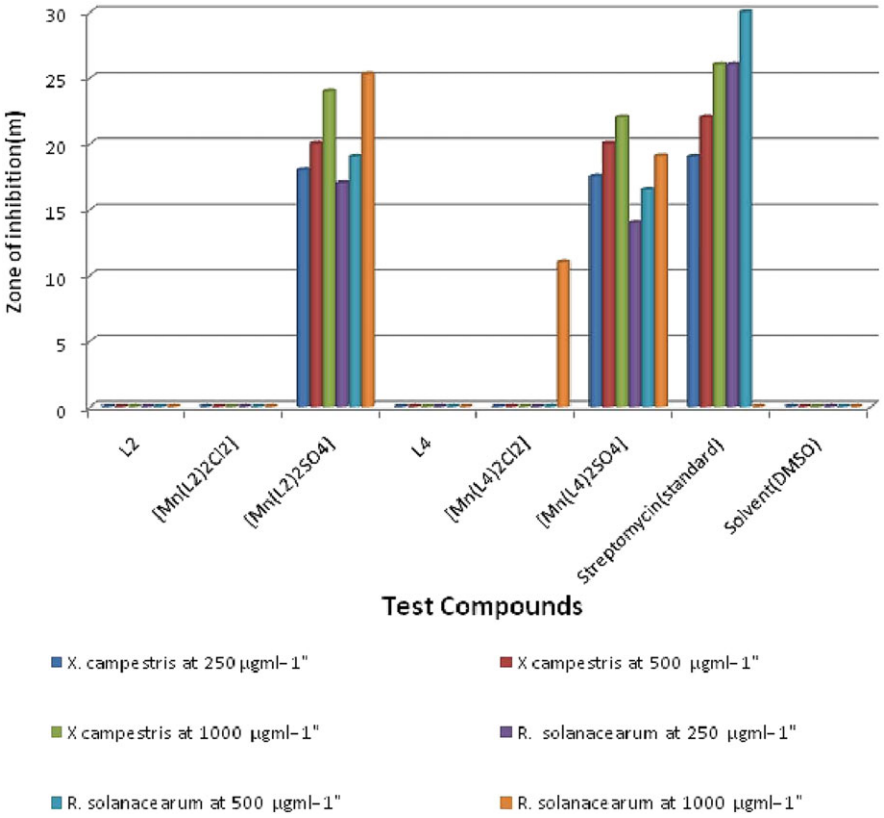

FIGURE 9 Activities of ligands L_2 and L_4 and their chloride and sulfato complexes against bacteria *X. campestris* pv. *campestris* (Xc) and *R. solanacearum* (Rs)

important to note that some of the metal chelates exhibit greater inhibitory effects than the parent ligands (Table 5). The increased activity of the metal chelates can be explained on the basis of chelation theory.[38] Some of the metal complexes exhibited greater activity than the commercial fungicide Bavistin (Figure 7). The data also indicated that the sulfato complexes of Mn(II) showed better activities than the chloro complexes. Further, the activities increased with increasing concentration of the compounds under investigation.

For fungus *M. phaseolena* (at a concentration of 1500 ppm) the activity order was: Bavistin (standard) > $[Mn(L_2)_2SO_4]$ > $[Mn(L_4)_2SO_4]$ > $[Mn(L_2)_2Cl_2]$ > $[Mn(L_1)_2SO_4]$ > $[Mn(L_3)_2SO_4]$ > $[Mn(L_3)_2Cl_2]$ > L_2 > $[Mn(L_1)_2Cl_2]$ > L_3 > L_1. Here the sulfato complexes with ligand L_2 and L_4 were found to be more active than the other complexes and ligands, while all the test compounds showed less activity than the commercial fungicide Bavistin.

The activity order for fungus *B. cinerea* (at a concentration of 1500 ppm) was found to be: $[Mn(L_1)_2SO_4]$ = $[Mn(L_2)_2Cl_2]$ = $[Mn(L_2)_2SO_4]$ = $[Mn(L_4)_2SO_4]$ ≈ $[Mn(L_3)_2SO_4]$ > $[Mn(L_3)_2Cl_2]$ > $[Mn(L_1)_2Cl_2]$ > $[Mn(L_4)_2Cl_2]$ > L_1 > Bavistin (standard) ≈ L_2. Here all the test compounds showed more activity than the commercial fungicide Bavistin (Figure 8).

The activity order for fungus *P. glomerata* (at a concentration of 1500 ppm) was found to be: Bavistin (standard) > $[Mn(L_4)_2SO_4]$ ≈ $[Mn(L_2)_2SO_4]$ ≈ $[Mn(L_3)_2SO_4]$ > $[Mn(L_1)_2SO_4]$ = $[Mn(L_2)_2Cl_2]$ = $[Mn(L_4)_2Cl_2]$ > $[Mn(L_1)_2Cl_2]$ ≈ $[Mn(L_3)_2Cl_2]$ > L_3 > L_2 > L_1. In this case the sulfato complexes with ligands L_2, L_3 and L_4 were found to be equally active as the other complexes and ligands but all the test compounds showed less activity than the commercial fungicide Bavistin.

4.9 | *In Vitro* screening for antibacterial activity

The data presented in Table 6 indicated that the sulfato complexes of Mn(II) with ligands L_2 and L_4 showed better activities against bacteria *X. campestris* pv. *campestris* as well as *R. solanacearum* than the parent ligands. The other ligands and complexes except $[Mn(L_4)_2Cl_2]$ did not show any activity against these two bacterial pathogens. The complex $[Mn(L_4)_2SO_4]$ was found to be more active than $[Mn(L_2)_2SO_4]$ against *X. campestris* pv. *campestris* at all concentrations, i.e. 250, 500 and 1000 $\mu g\ ml^{-1}$, but streptomycin (standard) showed better activities than the complexes at all concentrations (Figure 9).

5 | CONCLUSIONS

Different Mn(II) complexes having the general composition $Mn(L)_2X_2$ were synthesized and characterized using elemental analyses, molar conductance and magnetic moment

measurements, and mass, ^{1}H NMR, FT-IR, EPR and electronic spectral studies. The possible geometries of the complexes were assigned on the basis of EPR, electronic and FT-IR spectral data. The synthesized ligands and their complexes were screened for their antifungal activities against the fungi *M. phaseolina*, *B. cinerea* and *P. glomerata* and showed better results than the commercial fungicide Bavistin against *B. cinerea*. The sulfato complexes of Mn(II) with ligands L_2 and L_4 showed better activities against bacteria *X. campestris* pv. *campestris* and *R. solanacearum* than the parent ligands.

ACKNOWLEDGEMENTS

The authors are grateful to UGC, New Delhi for financial assistance, IIT Bombay for recording EPR spectra and IIT Delhi for recording NMR spectra. We are also grateful to Director, NBPGR, Pusa campus, New Delhi for providing facilities to conduct experiments for evaluating antimicrobial activities.

ORCID

Savita Bargujar http://orcid.org/0000-0002-1224-8391
Sulekh Chandra http://orcid.org/0000-0002-5439-5330

REFERENCES

[1] S. A. Hosseini-Yazdi, A. Mirzaahmadi, A. A. Khandar, V. Eigner, M. Dušek, F. Lotfipour, M. Mahdavi, S. Soltani, G. Dehghan, *Inorg. Chim. Acta* **2017**, *458*, 171.

[2] S. L. Sundaramurthy, G. Kannappan, P. Mahadevi, *J. Chem. Sci.* **2016**, *128*, 1113.

[3] N. Demirbas, S. A. Karaoglu, A. Demirbas, K. Sancak, *Eur. J. Med. Chem.* **2004**, *39*, 793.

[4] A. Mumtaz, T. Mahmud, M. R. Elsegood, G. W. Weaver, *J. Nucl. Med. Radiat. Ther.* **2016**, *7*, 310.

[5] A. A. Alomari, *J. Atoms Molecules* **2014**, *4*, 693.

[6] J. Wiecek, V. Dokorou, Z. Ciunik, D. Kovala-Demertzi, *Polyhedron* **2009**, *28*, 3298.

[7] M. A. Neelakantan, M. Esakkiamma, S. S. Mariappan, J. Dharmaraja, T. J. Kumar, *Ind. J. Pharm. Sci.* **2010**, *72*, 216.

[8] N. J. Suryawanshi, G. B. Pethe, S. G. Bhadange, A. S. Aswar, *J. Indian Chem. Soc.* **2013**, *90*, 1327.

[9] A. K. Sharma, S. Chandra, *Spectrochim. Acta A* **2011**, *81*, 424.

[10] J. Anandakumaran, M. L. Sundararajan, T. Jeyakumar, M. Nasir Uddin, *J. Am. Chem. Soc.* **2016**, *11*, 1.

[11] W. H. Mahmoud, R. G. Degadi, G. G. Mohamed, *Appl. Organometal. Chem.* **2016**, *30*, 221.

[12] N. J. Suryawanshi, G. B. Pethe, A. R. Yaul, A. S. Aswar, *Russian J. Gen. Chem.* **2016**, *86*, 901.

[13] U. E. Alan, M. M. Youssef, S. A. Shihry, *J. Mol. Struct.* **2009**, *936*, 213.

[14] A. R. Silva, V. Budarin, J. H. Clark, B. de Castro, C. Freire, *Carbon* **2005**, *43*, 2096.

[15] Y. K. Sharma, M. Karkwal, S. Uma, R. Nagarajan, *Polyhedron* **2009**, *28*, 205.

[16] M. Singh, V. Aggarwal, U. P. Singh, N. K. Singh, *Polyhedron* **2009**, *28*, 107.

[17] P. Merdy, E. Guillon, M. A. Plincourt, *New J. Chem.* **2002**, *26*, 1639.

[18] A. S. Mildwan, L. A. Loeb, *Adv. Inorg. Biochem.* **1981**, *3*, 103.

[19] H. A. Ewais, *J. Coord. Chem.* **2009**, *62*, 940.

[20] R. I. Kureshy, N. H. Khan, S. H. R. Abdi, P. Iyer, S. T. Patel, *Polyhedron* **1999**, *18*, 177.

[21] a) S. Chandra, L. K. Gupta, *Spectrochim. Acta A* **2005**, *61*, 269. b) N. Raman, S. Ravichandran, C. Thangaraja, *J. Chem. Sci.* **2004**, *116*, 215.

[22] S. Chandra, S. Bargujar, R. Nirwal, K. Qanungo, S. K. Sharma, *Spectrochim. Acta A* **2013**, *113*, 164.

[23] S. Chandra, S. Bargujar, R. Nirwal, N. Yadav, *Spectrochim. Acta A* **2013**, *106*, 91.

[24] K. P. Deepa, K. K. Aravindakshan, *Synth. React. Inorg. Met.-Org. Chem.* **2000**, *30*, 160.

[25] N. S. Youssef, K. H. Hegab, *Synth. React. Inorg. Met.-Org. Chem.* **2005**, *35*, 391.

[26] M. Tyagi, S. Chandra, P. Tyagi, *Spectrochim. Acta A* **2014**, *117*, 1.

[27] A. B. P. Lever, *Inorganic Electronic Spectroscopy*, 1st ed., Elsevier, Amsterdam **1968** 249.

[28] A. B. P. Lever, *Inorganic Electronic Spectroscopy*, Elsevier, Amsterdam **1984**.

[29] K. Nakamoto, *Infrared and Raman Spectra of Inorganic and Coordination Compounds*, 3rd ed., Wiley Interscience, New York **1978**.

[30] R. A. Ammar, A.-N. M. A. Alaghaz, M. E. Zayed, L. A. Al-Bedair, *J. Mol. Struct.* **2017**, *1141*, 368.

[31] S. Chandra, L. K. Gupta, *Spectrochim. Acta A* **2005**, *61*, 269.

[32] I. F. Orgel, *J. Chem. Phys.* **1855**, *23*, 1004.

[33] A. K. Maldhure, G. B. Pethe, A. R. Yaul, A. S. Aswar, *J. Korean Chem. Soc.* **2015**, *59*, 215.

[34] S. Chandra, K. Gupta, *Trans. Met. Chem.* **2002**, *27*, 329.

[35] HyperChem version 7.51, Hypercube Inc., USA.

[36] E. S. Freeman, B. J. Carroll, *J. Phys. Chem.* **1958**, *62*, 394.

[37] A. P. Mishra, M. Khare, *J. Ind. Chem. Soc.* **2000**, *77*, 367.

[38] S. Chandra, A. Kumar, *Spectrochim. Acta A* **2007**, *68*, 1410.

How to cite this article: Bargujar S, Chandra S, Chauhan R, Rajor HK, Bhardwaj J. Synthesis, spectroscopic evaluation, molecular modelling, thermal study and biological evaluation of manganese(II) complexes derived from bidentate N, O and N,S donor Schiff base ligands. *Appl Organometal Chem*. 2017;e4149. https://doi.org/10.1002/aoc.4149